28

On the Use of ^{203}Pb Imaging to Inform ^{212}Pb Dosimetry for $^{203/212}$Pb Image-Guided Alpha-Particle Therapy for Cancer

Stephen Graves, Mengshi Li, Dongyoul Lee, and Michael K. Schultz

28.1 Introduction

Emerging evidence suggests that receptor-targeted radionuclide therapy for cancer has the potential to be transformative for cancer patient care [1–15]. Alpha-particle radionuclide therapy (α-RT), in particular, is receiving considerable attention given the potential advantages of α-RT relative to (beta) β-RT. [1, 3, 5, 6, 16] Of these advantages (relative to β-emitters), higher linear-energy transfer (LET) (100 keV/μm) and resulting increases in primary and secondary ionizations along a relatively short path length in tissue is considered a primary advantage [3, 5, 11, 12, 15, 17]. The major underlying reason for this is that high LET radiation deposition over this short path length results in an increase in double-strand DNA breaks, which is thought to improve cytotoxicity via an improved relative biological effectiveness (RBE) when compared to β-RT. [18–21, 5, 16, 18–36] Of the radionuclides under investigation for α-RT, ^{225}Ac, ^{211}At, ^{212}Pb, ^{212}Bi, and ^{213}Bi have generated considerable enthusiasm [5, 16–36]. Of these, the only available elementally identical radionuclide pair for image-guided radionuclide therapy for cancer is ^{203}Pb/^{212}Pb, where gamma-emitting radionuclide ^{203}Pb can be used for single photon emission computed tomography (SPECT) and ^{212}Pb represents a potentially ideal radionuclide for specific classes of radiopharmaceuticals for delivering alpha particles to cancer cells.

Generator-produced ^{212}Pb ($t_{1/2}$ = 10.6 h; 100% β decay to alpha emitters ^{212}Bi and ^{212}Po) is rec-

S. Graves
Department of Radiology, University of Iowa, Iowa City, IA, USA

Department of Radiation Oncology, University of Iowa, Iowa City, IA, USA

Department of Biomedical Engineering, University of Iowa, Iowa City, IA, USA
e-mail: stephen-graves@uiowa.edu

M. Li · D. Lee
Perspective Therapeutics, Inc., Coralville, IA, USA

M. K. Schultz (✉)
Department of Radiology, University of Iowa, Iowa City, IA, USA

Department of Radiation Oncology, University of Iowa, Iowa City, IA, USA

Perspective Therapeutics, Inc., Coralville, IA, USA

Department of Pediatrics, University of Iowa, Iowa City, IA, USA

Department of Chemistry, University of Iowa, Iowa City, IA, USA
e-mail: michael-schultz@uiowa.edu

V. Prasad (ed.), *Beyond Becquerel and Biology to Precision Radiomolecular Oncology: Festschrift in Honor of Richard P. Baum*, https://doi.org/10.1007/978-3-031-33533-4_28

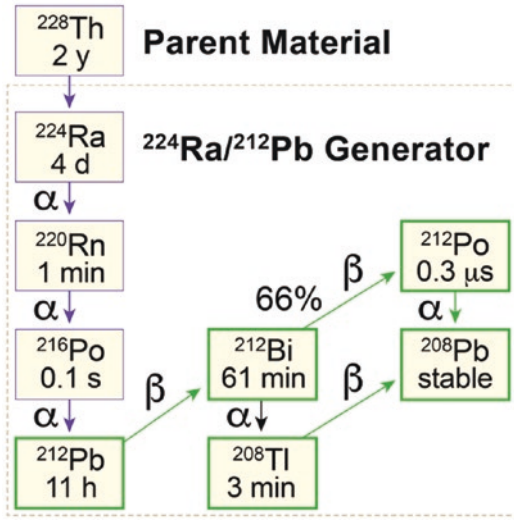

Fig. 28.1 Decay series for the production and use of ^{212}Pb for image-guided radionuclide therapy for cancer

ognized as a promising radionuclide for receptor-targeted α-RT (Fig. 28.1) [10, 33, 37–39]. However, α-decay cannot be used directly for molecular imaging. Therefore, a surrogate imaging radionuclide is required to perform complementary diagnostic imaging. The primary rationale for use of an elementally matched pair of radionuclides for this application is highlighted by recent comparisons of tumor and normal organ uptake of ^{68}Ga- and ^{90}Y-labeled small peptides in which measurable differences in pharmacokinetics were observed in in vivo biodistribution studies in mice [40]. Thus, for ^{212}Pb α-RT, the cyclotron-produced gamma(γ)-emitting radionuclide ^{203}Pb can be used as an elementally identical imaging surrogate [10, 33, 37, 38]. To wit, it can be expected that isotopes of the same element will have identical chemical and biochemical behaviors, adding confidence to predictions of ^{212}Pb α-RT outcomes using ^{203}Pb SPECT and SPECT/CT. However, in this context, uncertainties arise in these assumptions given the relationship between α-RT and imaging that must be considered in evaluation of ^{203}Pb SPECT. Stability of the ^{212}Pb-ligand complex and the potential for biological redistribution of daughter progeny gives rise to a potentially significant uncertainty in the use of ^{203}Pb SPECT for ^{212}Pb α-RT dosimetry. Here, we discuss factors relating to the introduction of these isotopes for image-guided radionuclide therapy for cancer.

28.2 ^{203}Pb SPECT/CT Imaging in Advance of ^{212}Pb α-RT

One of the potential advantages of ^{212}Pb-based alpha-emitting radiopharmaceuticals is the potential for using quantitative imaging by single photon emission computed tomography (SPECT) and computed tomography (CT) with ^{203}Pb-based surrogates to perform patient-specific dosimetry prior to therapy. It is anticipated that this could be most beneficial early in development process of new radiopharmaceuticals, such as in the preclinical setting and in early clinical trials (e.g., where organ doses can be monitored to develop understanding of the potential for other organ toxicities). SPECT imaging utilizes parallel hole collimation or pinhole collimation to obtain two-dimensional projections of the activity distribution within a patient. From these projected images and density information from CT imaging, a quantitative three-dimensional distribution of the radioactivity can be generated. Each quantitative image describes the activity distribution at a particular point in time, so multiple imaging time points are typically required to characterize the spatiotemporal characteristics of the radiopharmaceutical following administration.

Patient-specific pharmacokinetic data obtained through quantitation can be used to develop understanding by performing retrospective calculations regarding the absorbed dose to tumors and normal tissues. Dosimetry can enable patient-specific treatment optimization by delivering the maximum possible radiation dose to tumors without exceeding normal organ dose limits, which has the potential to improve the overall safety and efficacy of radiopharmaceutical therapies [41, 42]. Without dosimetric guidance, dose to normal tissues has been reported to vary by up to a factor of 5 per administered activity [43]. Based on these findings and observa-

tions, a dosimetrically informed therapy planning paradigm may be advantageous vs a "fixed activity" treatment strategy.

In some cases, dosimetry can be performed by administering a relatively low amount of the therapeutic radiopharmaceutical prior to treatment. This has been extensively demonstrated in the setting of radioiodine treatment for thyroid cancer—and this approach is now also the standard practice prior to treatment with iodine-131 labeled metaiodoguanidine (^{131}I-MIBG) for pheochromocytoma or paraganglioma [44, 45]. In other cases, a surrogate radiopharmaceutical is used to predict the biodistribution and pharmacokinetics of the therapeutic radiopharmaceutical. Use of ^{99m}Tc-labeled macroaggregated albumin (^{99m}Tc-MAA) to predict the distribution of ^{90}Y-microspheres is a prominent example, although it is known that the biodistribution of these two radiopharmaceuticals is somewhat dissimilar [46]. In the case of fractionated delivery of radiopharmaceutical therapy (routinely performed with ^{177}Lu-DOTATATE; 7.4 GBq per fraction for a total of 29.6 GBq), dosimetry can be performed directly following each treatment via SPECT CT imaging and medical physics analysis. This retrospective dosimetry approach allows for modification of subsequent administrations to target a specific cumulative dose. In all cases, it is important to note that the dose per administered activity can vary within a given subject based on differing metabolic states at the time of administration, or due to radiation-induced changes in patient physiology over the course of treatment. These observations suggest that a pretreatment dosimetric assessment repeated prior to each therapeutic fraction may be optimal.

In the case of image-guided radionuclide therapy using ^{212}Pb, an elementally identical gamma-emitting radionuclide (i.e., ^{203}Pb) can be employed for patient dosimetry. Practical considerations for quantitative SPECT imaging with ^{203}Pb are likely to parallel methods that have been developed for SPECT/CT following therapy with ^{177}Lu-based agents [47, 48]. Specific considerations include the collimator selection, the number of SPECT projections, the camera orbit trajectory, scatter window selection, dead time correction, attenuation correction, collimator detector response modeling, number of iterative updates during the reconstruction, and partial volume correction. One notable difference compared with methods developed for ^{177}Lu is that a high-energy collimator will likely be needed for use with ^{203}Pb due to the higher energy (279 keV vs 208 keV). In addition, it is possible that the size and makeup of scintillator crystals of the SPECT system may impact the efficiency of detection due the higher energy of the ^{203}Pb emission. A representative small animal image of ^{203}Pb-DOTATOC demonstrates the potential for ^{203}Pb-based SPECT CT (Fig. 28.2).

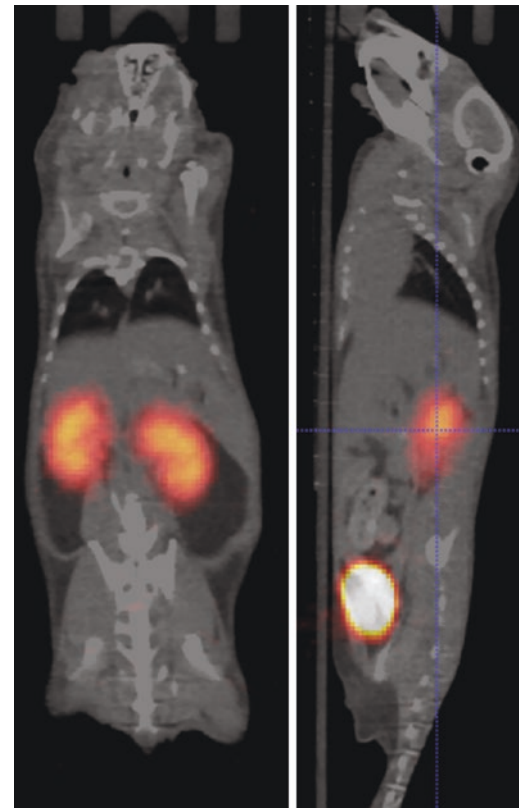

Fig. 28.2 ^{203}Pb-DOTATOC SPECT/CT in healthy ICR mice (HE pinhole collimator; Siemens Inveon)

28.3 Prediction of ^{212}Pb Dosimetry Based on ^{203}Pb Imaging

An elementally identical imaging surrogate (i.e., ^{203}Pb as a surrogate for ^{212}Pb) is potentially advantageous because the chemistry (and biochemistry) of nuclides of the same element are the same. However, potential uncertainties arise in the approach due to the subsequent nuclear transformations that generate ^{212}Pb radionuclide progeny in the ^{212}Pb decay series (Fig. 28.1). This scenario is common to other radiometals currently employed and under investigation for receptor-targeted alpha-particle therapy, including ^{225}Ac and ^{227}Th. A key distinguishing physical characteristic of these two radionuclides (i.e., difference from ^{212}Pb) is that their primary decay is directly by alpha-particle emission, while the ^{212}Pb nuclear transformation to radionuclide progeny ^{212}Bi occurs by beta-particle emission. This is important because the alpha-particle energy of the ^{225}Ac and ^{227}Th decay is undoubtedly sufficient to break the chemical bonds of the chelator-radiometal coupling of the daughter nuclei (i.e., ^{225}Ac–^{221}Fr and ^{227}Th–^{223}Ra). This phenomenon creates an immediate separation of the entire decay-series progeny from the site of the parent radionuclide (i.e., the chelator-ligand complex) that cannot be overcome. This phenomenon is potentially lessened in the case of ^{212}Pb, because the recoil energy imparted to the transforming nucleus is relatively small compared to alpha-particle-induced recoil energy [49]. Nonetheless, a critical parameter in assessing the uncertainty of modeling ^{212}Pb-based radionuclide therapy using ^{203}Pb imaging surrogates is an understanding of the potential for migration of ^{212}Pb decay series radionuclides from the site of ^{212}Pb decay. Within this context, the half-lives of ^{212}Po ($t_{1/2}$ 300 psec.) and ^{208}Tl ($t_{1/2}$ 3 min.) are sufficiently short such that understanding of the potential for ^{212}Bi to migrate from the site of ^{212}Pb decay is considered sufficient information to inform the uncertainty in using ^{203}Pb as a model for predicting ^{212}Pb alpha-particle dosimetry.

Within this context, one key parameter that remains in question is the kinetic stability of ^{212}Bi generated by the decay of ^{212}Pb within the chelator moieties employed for binding the radionuclides to the receptor-targeted ligands employed for delivering radiation to the tumor microenvironment. Extensive studies of the potential for differences in biodistribution of ^{212}Pb and ^{212}Bi (using the various chelator-ligand combinations for ^{212}Pb chelation and tumor delivery) have not been reported. The limited studies that have been reported explored the kinetic stability of ^{212}Bi generated by ^{212}Pb in the in vitro or in vivo setting. One study examined ^{203}Pb(II) and ^{206}Bi(III) chelate stability using a tetracarboxy chemical form of the chelator DOTA with no peptide ligand attached. This investigation showed that the chemical exchange of both Pb and Bi complexes with DOTA occur rather slowly in aqueous solution at physiologically relevant pH (pH 4–10). However, this study revealed that in the case of this tetra-carboxy DOTA derivative (free chelator without a peptide attached), approximately 30% of ^{212}Pb beta decays can result in the release of daughter ^{212}Bi from the chelator coupling, representing a potentially significant uncertainty that could be introduced with respect to pretreatment dosimetry that employs a ^{203}Pb-labeled agent as a surrogate for ^{212}Pb [50–52]. Further studies are required to develop a more detailed understanding of the chelator coupling with ^{212}Bi created by ^{212}Pb decay and it is anticipated that the stability of the ^{212}Pb-chelator complexes will be chelator-specific. An examination of this type for specific chelator-modified peptide conjugates will be needed to develop a more empirical understanding for individual radiopharmaceuticals.

A majority of energy released during the ^{212}Pb decay chain arises via alpha emissions of ^{212}Bi ($t_{1/2}$ 61 min) and that of the short-lived ^{212}Bi daughter, ^{212}Po ($t_{1/2}$: 0.3 μs). The radioactive half-life of ^{212}Bi may be long enough to redistribute within the body according to its own pharmacokinetics depending on the tissue type—and depending on whether the bismuth atom is released within a cell or in the extracellular environment. Reported pharmacokinetic data provides some information regarding the biological fate of radioactive bismuth ions in humans. As is

the case for numerous other elements, the International Commission on Radiological Protection (ICRP) has created a pharmacokinetic model for bismuth based on human data from accidental or intentional exposures to radiobismuth [53]. This model is reproduced in Fig. 28.3 with transfer rate constants specified in Table 28.1. Most forms of bismuth (those prone to ionic dissociation) clear rapidly from the blood with significant accumulation in the kidneys and liver. With consideration given toward bismuth released within tumors, activity that is released into extracellular fluid (represented by the rapid turnover compartment in Fig. 28.3) will clear quickly ($k = 66\ d^{-1}$) into the plasma, and subsequently into the liver ($k = 30\ d^{-1}$) and renal structures ($k = 36\ d^{-1}$). For this reason, dose to tumors may be overestimated by ^{203}Pb imaging, and dose to other normal tissues may be underestimated. The potential for new chelator technologies to be introduced that protect the integrity of the daughter-chelator coupling post-decay of ^{212}Pb has the potential to mitigate this uncertainty and more research in this area is needed.

In order to estimate the degree of systematic error from ^{203}Pb-based predictions of ^{212}Pb biodistribution, the pharmacokinetic model described by Fig. 28.3 and Table 28.1 was implemented in a MatLab script. Bismuth ions were assumed to be generated in various subcompartments (soft tissue, kidneys, liver, blood), and the fate of ions at the time of radioactive decay were tallied. Organ-specific time activity curves for the case where ions are released within the tumor extracellular compartment is shown in Fig. 28.4. Transfer of activity from the extracellular soft tissue space to the plasma occurs rapidly, followed by localization in the kidneys and liver within approximately 1 h. Integration of these time activity curves reveals that 50% of released bismuth ions would decay prior to leaving the soft tissue compartment, while the blood, liver, and kidneys receive 8%, 13%, and 15% of decays, respectively. In the case of bismuth released while the radiopharmaceutical is in the blood, only 10% of ^{212}Bi decays occur prior to clearance from the blood, while the liver, kidneys, and other soft tissues receive 17%, 19% and 37% of decays, respectively. Other combinations of "source" and "target" organs are listed in Table 28.2. Data generated from this pharmacokinetic modeling, combined with information regarding the fraction of ^{212}Bi daughters that are released from a particular chelator, allows for improved accuracy when extrapolating from ^{203}Pb imaging.

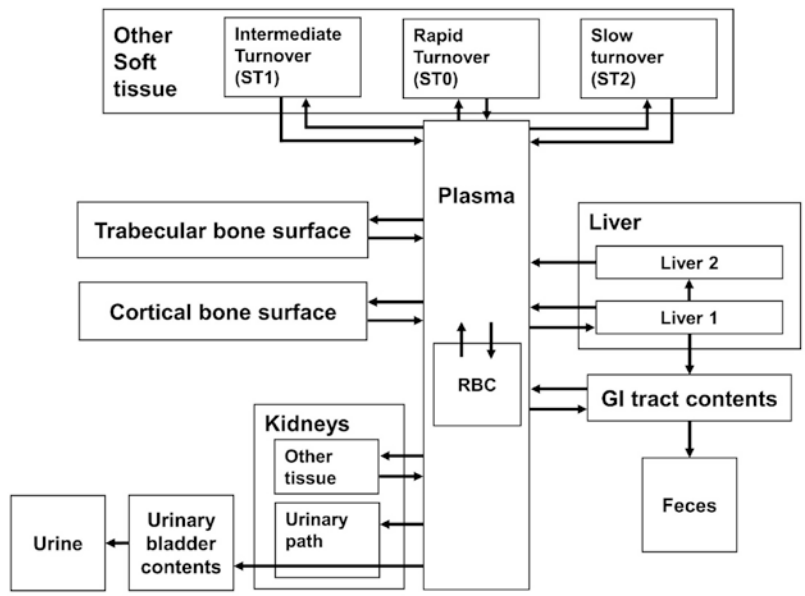

Fig. 28.3 Pharmacokinetic model of bismuth in the body, reproduced with permission from ICRP 137 [53]

Table 28.1 Transfer coefficients for bismuth pharmacokinetic model. Reproduced with permission from ICRP 137 [53]

From	To	Transfer coefficient (d^{-1})
Plasma	Urinary bladder contents	20
Plasma	Right colon contents	4
Plasma	RBC	0.5
Plasma	ST0	300
Plasma	ST1	4.2
Plasma	ST2	1.3
Plasma	Liver 1	30
Plasma	Urinary path (kidneys)	30
Plasma	Other kidney tissue	5
Plasma	Cortical bone surface	2.5
Plasma	Trabecular bone surface	2.5
RBC	Plasma	0.173
ST0	Plasma	66
ST1	Plasma	0.0347
ST2	Plasma	0.00116
Liver 1	Small intestine contents	0.208
Liver 1	Liver 2	0.139
Liver 2	Plasma	0.0693
Urinary path (kidneys)	Urinary bladder contents	0.693
Other kidney tissues	Plasma	0.139
Cortical bone surface	Plasma	0.0347
Trabecular bone surface	Plasma	0.0347

If the fraction of bismuth ions released (f) is known, a generalized formalism can be devised to account for this redistribution effect by correcting ^{203}Pb-derived time-integrated activities:

$$\tilde{A}(r_i) = (1-f)\tilde{A}_{raw}(r_i) + f\sum_{r_S}\tilde{A}_{raw}(r_s)\psi(r_i \leftarrow r_s)$$

In this formalism, $\tilde{A}_{raw}(r_i)$ is the time-integrated activity for a given organ (r_i) without correcting for the redistribution effect, and $\tilde{A}(r_i)$

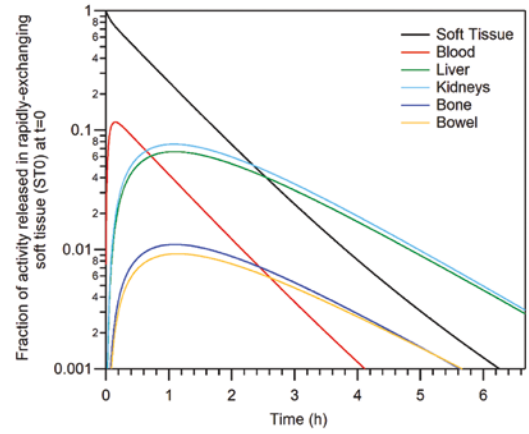

Fig. 28.4 Time-activity curves following a release of free ^{212}Bi within the extracellular soft tissue space, such as what would be observed with non-internalized tumor uptake of a radiopharmaceutical

is the corrected time-integrated activity for that organ. The fractional transfer of time-integrated activity from a given source organ (r_s) to the organ of interest (r_i) is represented by the product of f and $\psi(r_i \leftarrow r_s)$ (Table 28.2), where $\psi(r_i \leftarrow r_s)$ describes the probability of a given bismuth ion decaying in r_i when it was released from r_s. More sophisticated microdosimetric correction factors could potentially be developed if sub-organ pharmacokinetic models were utilized in a similar fashion to what has been described here. Once $\tilde{A}(r_i)$ is determined for each tissue type, patient-specific dosimetry can proceed according to MIRD methods [54]. It is worth noting that within this formalism the release of activity within tumors should be treated separately from other soft tissues in the body, and that the additive correction—$\sum_{r_S}\tilde{A}_{raw}(r_s)\psi(r_i \leftarrow r_s)$—should distribute time-integrated activity uniformly over all soft tissues, including tumors. Also notable is that this methodology could potentially be extended to ^{225}Ac-based radiopharmaceuticals to estimate dose due to redistribution of daughters (^{211}Fr, ^{207}At, ^{213}Bi). In this way, a more detailed understanding of the potential off-target dosimetry can be obtained that can be used for more precise image-guided radionuclide therapy treatment planning.

Table 28.2 Fraction of energy deposited in normal structures as a function of where ^{212}Bi is released. When ^{212}Bi is released in liver, kidneys, and intracellular soft tissue compartments (ST1, ST2), the biological redistribution of ^{212}Bi is negligible prior to decay. Consideration should be given to ^{212}Bi that is released in the extracellular soft-tissue compartment (ST0) as well as ^{212}Bi that is released in the blood plasma

	Fraction of energy deposited from free ^{212}Bi						
Source compartment	Blood	Soft tissue	Liver	Kidneys	Bone	Bowel	Urine
Plasma	0.096	0.372	0.168	0.191	0.028	0.025	0.120
Rapid turnover tissue (ST0)	0.077	0.497	0.134	0.153	0.023	0.020	0.096
Intermediate turnover tissue (ST1)	0.000	0.999	0.000	0.000	0.000	0.000	0.000
Slow turnover tissue (ST2)	0.000	1.000	0.000	0.000	0.000	0.000	0.000
Liver 1	0.000	0.000	0.988	0.000	0.000	0.012	0.000
Liver 2	0.000	0.002	0.996	0.001	0.000	0.000	0.000
Urinary path, kidney	0.000	0.000	0.000	0.960	0.000	0.000	0.040
Other kidney tissue	0.001	0.003	0.001	0.993	0.000	0.000	0.001
Bone	0.000	0.001	0.000	0.000	0.998	0.000	0.000

28.4 Summary and Future Directions

Alpha-emitting radiopharmaceutical therapy shows promise for improving the therapeutic efficacy of existing and future targeting ligands by limiting off-target irradiation and by preempting many cell survival mechanisms (e.g., DNA repair, hypoxia). In addition to the potency of alpha radiation, dosimetry-guided therapies have been shown to be potentially safer and more effective than RPT administration under a fixed-activity paradigm. Among the candidates of alpha-emitting radioisotopes, ^{212}Pb shows promise for use under a theranostic paradigm, whereby ^{203}Pb can be used for dosimetry and treatment planning.

In this chapter, we have presented an approach for accurately estimating the dosimetry of ^{212}Pb-based radiopharmaceuticals using ^{203}Pb as a surrogate. Moving forward, it will be necessary to establish more precisely the uncertainties arising under this paradigm and to experimentally validate the model used to predict the redistribution of ^{212}Bi following the decay of ^{212}Pb. One way to approach this problem would be to perform comparative biodistribution studies, whereby a ^{212}Pb-bearing compound is administered to a mouse that is sacrificed at specified time points postinjection. Tissue samples would be acquired promptly, and quantitative gamma spectrometry could be performed to differentiate between the location of ^{212}Pb and ^{212}Bi (unsupported vs supported) (and progeny) in the body. The gamma emission energies of ^{212}Pb (E_γ: 239 keV, 43.6%), ^{212}Bi (E_γ: 727 keV, 6.7%), ^{212}Po (E_γ: 570 keV, 2%), and ^{208}Tl (E_γ: 583 keV, 85%) are sufficiently distinct and abundant as to enable quantitative energy-peak spectroscopic measurements by sodium iodide solid scintillation detectors and by high-purity germanium detector. The challenging aspects of this experiment are (1) minimizing the time between animal sacrifice and spectroscopic measurements, and (2) appropriately modeling the decay of unsupported ^{212}Bi, and ingrowth of ^{212}Bi in tissues where ^{212}Pb is present. Careful uncertainty analysis will be required when considering the alteration of redistribution dosimetric modeling parameters.

Experiments are also needed to elucidate the toxicity of bioconjugated and free ^{212}Bi in tissues of interest, normalized to tissue mean dose. It has been shown that microdosimetric factors, such as what organ sub-structure the radioactivity resides in, can substantially alter organ-level toxicity [55]. Therefore, on a per-radiopharmaceutical basis, it may be important to consider the differential distribution of free ^{212}Bi ions and radiopharmaceutical-bound activity.

Research productivity in the field of αRPT is growing rapidly, as evidenced by the ~ten-fold increase in publications per year over the last

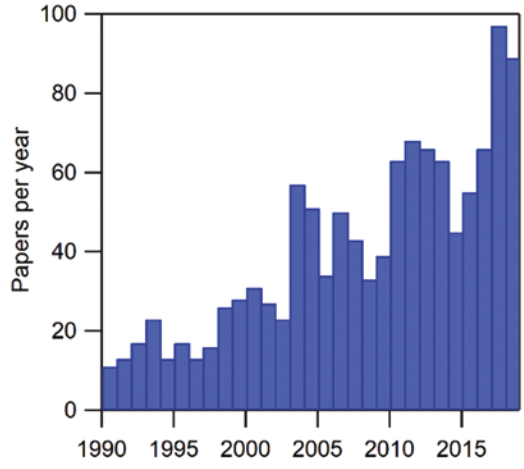

Fig. 28.5 PubMed results by year for the search terms ^{212}Pb, ^{225}Ac, ^{212}Bi, ^{213}Bi, ^{211}At, and ^{227}Th

30 years (Fig. 28.5). Human therapy studies have shown promising preliminary results, and the field of αRPT is benefiting from the development of new and innovative beta-emitting radiopharmaceutical therapies. We foresee continued growth in research productivity in this area, as well as improved patient care standards as technologies progress. Lead-212 is likely to play a key role in the progress toward personalized αRPT.

References

1. Bartlett M. From the inside out: radionuclide radiation therapy. Australas Phys Eng Sci Med. 2016;39(2):357–9. https://doi.org/10.1007/s13246-016-0455-9.
2. Hardiansyah D, Guo W, Kletting P, Mottaghy FM, Glatting G. Time-integrated activity coefficient estimation for radionuclide therapy using PET and a pharmacokinetic model: a simulation study on the effect of sampling schedule and noise. Med Phys. 2016;43(9):5145. https://doi.org/10.1118/1.4961012.
3. Iagaru AH, Mittra E, Colletti PM, Jadvar H. Bone-targeted imaging and radionuclide therapy in prostate cancer. J Nucl Med. 2016;57(Suppl 3):19S–24S. https://doi.org/10.2967/jnumed.115.170746. PubMed PMID: 27694165; PMCID: PMC5093914.
4. Jin ZH, Furukawa T, Degardin M, Sugyo A, Tsuji AB, Yamasaki T, Kawamura K, Fujibayashi Y, Zhang MR, Boturyn D, Dumy P, Saga T. alphaV-beta3 integrin-targeted radionuclide therapy with 64Cu-cyclam-RAFT-c(-RGDfK-)4. Mol Cancer Ther. 2016;15(9):2076–85. https://doi.org/10.1158/1535-7163.MCT-16-0040.
5. Kratochwil C, Giesel FL, Stefanova M, Benesova M, Bronzel M, Afshar-Oromieh A, Mier W, Eder M, Kopka K, Haberkorn U. PSMA-targeted radionuclide therapy of metastatic castration-resistant prostate cancer with 177Lu-labeled PSMA-617. J Nucl Med. 2016;57(8):1170–6. https://doi.org/10.2967/jnumed.115.171397.
6. Kwekkeboom DJ, Krenning EP. Peptide receptor radionuclide therapy in the treatment of neuroendocrine tumors. Hematol Oncol Clin North Am. 2016;30(1):179–91. https://doi.org/10.1016/j.hoc.2015.09.009.
7. Li W, Liu Z, Li C, Li N, Fang L, Chang J, Tan J. Radionuclide therapy using (1)(3)(1)I-labeled anti-epidermal growth factor receptor-targeted nanoparticles suppresses cancer cell growth caused by EGFR overexpression. J Cancer Res Clin Oncol. 2016;142(3):619–32. https://doi.org/10.1007/s00432-015-2067-2.
8. Lo Russo G, Pusceddu S, Prinzi N, Imbimbo M, Proto C, Signorelli D, Vitali M, Ganzinelli M, Maccauro M, Buzzoni R, Seregni E, de Braud F, Garassino MC. Peptide receptor radionuclide therapy: focus on bronchial neuroendocrine tumors. Tumour Biol. 2016;37:12991. https://doi.org/10.1007/s13277-016-5258-9.
9. Nonnekens J, van Kranenburg M, Beerens CE, Suker M, Doukas M, van Eijck CH, de Jong M, van Gent DC. Potentiation of peptide receptor radionuclide therapy by the PARP inhibitor olaparib. Theranostics. 2016;6(11):1821–32. https://doi.org/10.7150/thno.15311. PubMed PMID: 27570553; PMCID: PMC4997239.
10. Norain A, Dadachova E. Targeted radionuclide therapy of melanoma. Semin Nucl Med. 2016;46(3):250–9. https://doi.org/10.1053/j.semnuclmed.2015.12.005.
11. Otte A. Neuroendocrine tumors: peptide receptors radionuclide therapy (PRRT). Hell J Nucl Med. 2016;19(2):182. https://doi.org/10.1967/s0024499100378.
12. Takahashi A, Miwa K, Sasaki M, Baba S. A Monte Carlo study on (223)Ra imaging for unsealed radionuclide therapy. Med Phys. 2016;43(6):2965–74. https://doi.org/10.1118/1.4948682.
13. Weber WA, Morris MJ. Molecular imaging and targeted radionuclide therapy of prostate cancer. J Nucl Med. 2016;57(Suppl 3):3S–5S. https://doi.org/10.2967/jnumed.116.175497.
14. Werner RA, Lapa C, Ilhan H, Higuchi T, Buck AK, Lehner S, Bartenstein P, Bengel F, Schatka I, Muegge DO, Papp L, Zsoter N, Grosse-Ophoff T, Essler M, Bundschuh RA. Survival prediction in patients undergoing radionuclide therapy based on intratumoral somatostatin-receptor heterogeneity. Oncotarget. 2016;8:7039. https://doi.org/10.18632/oncotarget.12402.
15. Zukotynski K, Jadvar H, Capala J, Fahey F. Targeted radionuclide therapy: practical applications and future prospects. Biomark Cancer. 2016;8(Suppl 2):35–8.

https://doi.org/10.4137/BIC.S31804. PubMed PMID: 27226737; PMCID: PMC4874742.
16. Kratochwil C, Bruchertseifer F, Giesel FL, Weis M, Verburg FA, Mottaghy F, Kopka K, Apostolidis C, Haberkorn U, Morgenstern A. 225Ac-PSMA-617 for PSMA targeting alpha-radiation therapy of patients with metastatic castration-resistant prostate cancer. J Nucl Med. 2016. Epub 2016/07/09.;57:1941. https://doi.org/10.2967/jnumed.116.178673.
17. Wild D, Frischknecht M, Zhang H, Morgenstern A, Bruchertseifer F, Boisclair J, Provencher-Bolliger A, Reubi JC, Maecke HR. Alpha- versus beta-particle radiopeptide therapy in a human prostate cancer model (213Bi-DOTA-PESIN and 213Bi-AMBA versus 177Lu-DOTA-PESIN). Cancer Res. 2011;71(3):1009–18. https://doi.org/10.1158/0008-5472.CAN-10-1186.
18. Hobbs RF, Howell RW, Song H, Baechler S, Sgouros G. Redefining relative biological effectiveness in the context of the EQDX formalism: implications for alpha-particle emitter therapy. Radiat Res. 2014;181(1):90–8. https://doi.org/10.1667/RR13483.1. PubMed PMID: 24502376; PMCID: PMC3984880.
19. Sgouros G. Alpha-particles for targeted therapy. Adv Drug Deliv Rev. 2008;60(12):1402–6. https://doi.org/10.1016/j.addr.2008.04.007.
20. Sgouros G, Hobbs RF, Song H. Modelling and dosimetry for alpha-particle therapy. Curr Radiopharm. 2011;4(3):261–5. PubMed PMID: 22201712; PMCID: PMC4332831.
21. Sgouros G, Roeske JC, McDevitt MR, Palm S, Allen BJ, Fisher DR, Brill AB, Song H, Howell RW, Akabani G, Bolch WE, Brill AB, Fisher DR, Howell RW, Meredith RF, Sgouros G, Wessels BW, Zanzonico PB. MIRD pamphlet No. 22 (abridged): radiobiology and dosimetry of alpha-particle emitters for targeted radionuclide therapy. J Nucl Med. 2010;51(2):311–28 . Epub 2010/01/19. https://doi.org/10.2967/jnumed.108.058651.
22. Akabani G, Kennel SJ, Zalutsky MR. Microdosimetric analysis of alpha-particle-emitting targeted radiotherapeutics using histological images. J Nucl Med. 2003;44(5):792–805.
23. Behr TM, Behe M, Jungclas H, Jungclas H, Becker W, Sgouros G. Higher relative biological efficiency of alpha-particles: in vitro veritas, in vitro vanitas? Eur J Nucl Med. 2001;28(9):1435–6.
24. Behr TM, Behe M, Stabin MG, Wehrmann E, Apostolidis C, Molinet R, Strutz F, Fayyazi A, Wieland E, Gratz S, Koch L, Goldenberg DM, Becker W. High-linear energy transfer (LET) alpha versus low-LET beta emitters in radioimmunotherapy of solid tumors: therapeutic efficacy and dose-limiting toxicity of 213Bi- versus 90Y-labeled CO17-1A Fab' fragments in a human colonic cancer model. Cancer Res. 1999;59(11):2635–43.
25. Elgqvist J, Frost S, Pouget JP, Albertsson P. The potential and hurdles of targeted alpha therapy—clinical trials and beyond. Front Oncol. 2014;3:324. https://doi.org/10.3389/fonc.2013.00324. PubMed PMID: 24459634; PMCID: PMC3890691.
26. Hauck ML, Larsen RH, Welsh PC, Zalutsky MR. Cytotoxicity of alpha-particle-emitting astatine-211-labelled antibody in tumour spheroids: no effect of hyperthermia. Br J Cancer. 1998;77(5):753–9. PubMed PMID: 9514054; PMCID: PMC2149964
27. Humm JL, Chin LM. A model of cell inactivation by alpha-particle internal emitters. Radiat Res. 1993;134(2):143–50.
28. Jurcic JG, Larson SM, Sgouros G, McDevitt MR, Finn RD, Divgi CR, Ballangrud AM, Hamacher KA, Ma D, Humm JL, Brechbiel MW, Molinet R, Scheinberg DA. Targeted alpha particle immunotherapy for myeloid leukemia. Blood. 2002;100(4):1233–9.
29. Kim YS, Brechbiel MW. An overview of targeted alpha therapy. Tumour Biol. 2012;33(3):573–90. https://doi.org/10.1007/s13277-011-0286-y.
30. Kratochwil C, Giesel FL, Bruchertseifer F, Mier W, Apostolidis C, Boll R, Murphy K, Haberkorn U, Morgenstern A. (2)(1)(3)bi-DOTATOC receptor-targeted alpha-radionuclide therapy induces remission in neuroendocrine tumours refractory to beta radiation: a first-in-human experience. Eur J Nucl Med Mol Imaging. 2014;41(11):2106–19. https://doi.org/10.1007/s00259-014-2857-9. PubMed PMID: 25070685; PMCID: PMC4525192.
31. Macklis RM, Kinsey BM, Kassis AI, Ferrara JL, Atcher RW, Hines JJ, Coleman CN, Adelstein SJ, Burakoff SJ. Radioimmunotherapy with alpha-particle-emitting immunoconjugates. Science (New York, NY). 1988;240(4855):1024–6. Epub 1988/05/20.
32. McDevitt MR, Sgouros G, Finn RD, Humm JL, Jurcic JG, Larson SM, Scheinberg DA. Radioimmunotherapy with alpha-emitting nuclides. Eur J Nucl Med. 1998;25(9):1341–51.
33. Miao Y, Hylarides M, Fisher DR, Shelton T, Moore H, Wester DW, Fritzberg AR, Winkelmann CT, Hoffman T, Quinn TP. Melanoma therapy via peptide-targeted {alpha}-radiation. Clin Cancer Res. 2005;11(15):5616–21. Epub 2005/08/03. https://doi.org/10.1158/1078-0432.ccr-05-0619.
34. Sgouros G, Song H. Cancer stem cell targeting using the alpha-particle emitter, 213Bi: mathematical modeling and feasibility analysis. Cancer Biother Radiopharm. 2008;23(1):74–81. https://doi.org/10.1089/cbr.2007.0408. PubMed PMID: 18298331; PMCID: PMC2977973.
35. Wadas TJ, Pandya DN, Solingapuram Sai KK, Mintz A. Molecular targeted alpha-particle therapy for oncologic applications. AJR Am J Roentgenol. 2014;203(2):253–60. https://doi.org/10.2214/AJR.14.12554. PubMed PMID: 25055256; PMCID: PMC4490786.
36. Zalutsky MR. Targeted alpha-particle therapy of microscopic disease: providing a further rationale for clinical investigation. J Nucl Med. 2006;47(8):1238–40.

37. Miao Y, Figueroa SD, Fisher DR, Moore HA, Testa RF, Hoffman TJ, Quinn TP. 203Pb-labeled alpha-melanocyte-stimulating hormone peptide as an imaging probe for melanoma detection. J Nucl Med. 2008;49(5):823–9. Epub 2008/04/17. https://doi.org/10.2967/jnumed.107.048553.
38. Miao Y, Quinn TP. Peptide-targeted radionuclide therapy for melanoma. Critical Rev Oncol. 2008;67(3):213–28. Epub 2008/04/05. https://doi.org/10.1016/j.critrevonc.2008.02.006.
39. Martin ME, Sue O'Dorisio M, Leverich WM, Kloepping KC, Walsh SA, Schultz MK. "click"-cyclized (68)Ga-labeled peptides for molecular imaging and therapy: synthesis and preliminary in vitro and in vivo evaluation in a melanoma model system. Recent Results Cancer Res. 2013;194:149–75. https://doi.org/10.1007/978-3-642-27994-2_9. PubMed PMID: 22918759; PMCID: PMC3799893.
40. Fani M, Maecke HR. Radiopharmaceutical development of radiolabelled peptides. Eur J Nucl Med Mol Imaging. 2012;39(Suppl 1):S11–30. Epub 2012/03/06. https://doi.org/10.1007/s00259-011-2001-z.
41. Strigari L, Konijnenberg M, Chiesa C, Bardies M, Du Y, Gleisner KS, Lassmann M, Flux G. The evidence base for the use of internal dosimetry in the clinical practice of molecular radiotherapy. Eur J Nucl Med Mol Imaging. 2014;41(10):1976–88.
42. Garske-Román U, Sandström M, Baron KF, Lundin L, Hellman P, Welin S, Johansson S, Khan T, Lundqvist H, Eriksson B. Prospective observational study of 177 Lu-DOTA-octreotate therapy in 200 patients with advanced metastasized neuroendocrine tumours (NETs): feasibility and impact of a dosimetry-guided study protocol on outcome and toxicity. Eur J Nucl Med Mol Imaging. 2018;45(6):970–88.
43. Menda Y, Madsen MT, O'Dorisio TM, Sunderland JJ, Watkins GL, Dillon JS, Mott SL, Schultz MK, Zamba GK, Bushnell DL. 90Y-DOTATOC dosimetry–based personalized peptide receptor radionuclide therapy. J Nucl Med. 2018;59(11):1692–8.
44. Pryma DA, Chin BB, Noto RB, Dillon JS, Perkins S, Solnes L, Kostakoglu L, Serafini AN, Pampaloni MH, Jensen J. Efficacy and safety of high-specific-activity 131I-MIBG therapy in patients with advanced pheochromocytoma or paraganglioma. J Nucl Med. 2019;60(5):623–30.
45. Lassmann M, Reiners C, Luster M. Dosimetry and thyroid cancer: the individual dosage of radioiodine. Endocr Relat Cancer. 2010;17(3):R161–R72.
46. Kim SP, Cohalan C, Kopek N, Enger SA. A guide to 90Y radioembolization and its dosimetry. Phys Med. 2019;68:132–45.
47. Dewaraja YK, Frey EC, Sgouros G, Brill AB, Roberson P, Zanzonico PB, Ljungberg M. MIRD pamphlet no. 23: quantitative SPECT for patient-specific 3-dimensional dosimetry in internal radionuclide therapy. J Nucl Med. 2012;53(8):1310–25.
48. Ljungberg M, Celler A, Konijnenberg MW, Eckerman KF, Dewaraja YK, Sjögreen-Gleisner K. MIRD pamphlet no. 26: joint EANM/MIRD guidelines for quantitative 177Lu SPECT applied for dosimetry of radiopharmaceutical therapy. J Nucl Med. 2016;57(1):151–62.
49. Azure MT, Archer RD, Sastry KS, Rao DV, Howell RW. Biological effect of lead-212 localized in the nucleus of mammalian cells: role of recoil energy in the radiotoxicity of internal alpha-particle emitters. Radiat Res. 1994;140(2):276–83. Epub 1994/11/01. PubMed PMID: 7938477; PMCID: PMC3321059.
50. Gansow OA, Wu C, Goldenberg D. Advanced methods for radiolabeling monoclonal antibodies with therapeutic radionuclides. In: Cancer therapy with radiolabeled antibodies. Boca Raton, FL: CRC; 1995. p. 63–76.
51. Gansow O, Brechbiel M, Pippin C, McMurry T, Lambrecht R, Colcher D, Schlom J, Roselli M, Strand M, Huneke R. Lead and bismuth complexes of functionalized dtpa ligands and of the polyazacycloalkane-n-acetic acid dota-utility for radioimmunoimaging and radioimmunotherapy. Antib Immunoconjug Radiopharm. 1991;4(4):413–25.
52. Mirzadeh S, Kumar K, Gansow OA. The chemical fate of 212Bi-DOTA formed by β-decay of 212Pb (DOTA) 2. Radiochim Acta. 1993;60(1):1–10.
53. Paquet F, Bailey M, Leggett RW, Lipsztein J, Marsh J, Fell T, Smith T, Nosske D, Eckerman KF, Berkovski V. ICRP publication 137: occupational intakes of radionuclides: part 3. Ann ICRP. 2017;46(3–4):1–486.
54. Wessels BW, Konijnenberg MW, Dale RG, Breitz HB, Cremonesi M, Meredith RF, Green AJ, Bouchet LG, Brill AB, Bolch WE. MIRD pamphlet No. 20: the effect of model assumptions on kidney dosimetry and response—implications for radionuclide therapy. J Nucl Med. 2008;49(11):1884–99.
55. Hobbs RF, Song H, Huso DL, Sundel MH, Sgouros G. A nephron-based model of the kidneys for macro-to-micro α-particle dosimetry. Phys Med Biol. 2012;57(13):4403.